

NUMERICAL SIMULATION OF 3D FLAPPING WING BASED ON CHIMERA METHOD

Wenqing Yang, Bifeng Song, Wenping Song

School of Aeronautics, Northwestern Polytechnical University, Xi'an, P.R. China, 710072

Keywords: flapping wing; CFD; chimera method; 3D; NS equations

Abstract

The aerodynamic characteristics of flapping wing are investigated by solving the 3D Euler/Navier-Stokes equations based on the chimera method. The spatial discretization is characterized by a second-order cell-center method for finite volumes. A five-stage Runge-Kutta scheme is employed to achieve convergence of the solution by integration with respect to time. For unsteady flows an implicit dual time-stepping scheme is used. Implicit residual smoothing is employed to accelerate convergence. The Baldwin-Lomax algebraic turbulent model is applied for calculating the turbulence flows. The grid system is based on the chimera method which includes the motion wing grid and stationary background grid. Chimera grid is chosen for it's easy to deal with complex configuration and moving bodies. Besides, an efficient method, namely distance-decreasing searching method, is developed to apply on the hole-cutting and the interpolation cells searching of chimera grid preprocessing. Based on these numerical methods, comparison between the results of Euler and Reynolds Average Navier-Stokes (RANS) equations is given. Then, the effect of reduced frequency, angle of attack, flapping angle, twisting angle, and airfoil of cross section are researched. The result shows that the lift and thrust coefficients get by RANS is lower than the Euler equations because of viscosity. And the result accord with the actual situation logically. The increasing of angle of attack can increase the lift coefficient, but decrease the thrust coefficient. The increasing of reduce frequency can increase the thrust coefficient, but affect average lift coefficient slightly, just increase the peak value

range of lift coefficient. The increasing of flapping angle affects the lift and thrust coefficient similarly as the increasing reduced frequency. The increasing of twisting angle can decrease the peak value range of lift coefficient and decrease the thrust coefficient at the condition of $\Phi=90^\circ$. The airfoil thickness has little effect on lift coefficient, but has obvious effect on thrust coefficients. The relationship between airfoil thickness and thrust coefficient is not monotony. Too thin or too thick airfoils both can not get big thrust coefficient.

1 Introduction

Birds flap wings up and down to produce lift and thrust at the same time. People are highly interested in researching of the flapping flight, for the entire flying birds take the flapping wing as their way to flight. The motions of bird's flight are composed from three important motions: flapping, twisting and folding. The smart mixture of three motions makes birds outstanding flyers. The recent interest in flapping wing air vehicle is motivated by the notion that flapping wing may offer some unique aerodynamic advantages over a fixed wing solution. People have done much research work on flapping wing by experimental, theoretical, and computational ways.

The numerical simulations of solving Euler/Navier-Stokes equations are used more and more in the flapping wing research for its high precision. Neef and Hummel [1] have investigated plunging and pitching NACA0012 airfoil in 2D and 3D flow. They solved the Euler equations for a rectangular wing in a sinusoidal flapping and twisting motion. Tuncer and Platzer [2] used a 2D compressible Navier-

Stokes/potential solver to predict thrust generation in flapping/stationary airfoil combinations in tandem. Lin and Hu [3] developed a 3D Euler/Navier-Stokes solver for simulation plunging/pitching NACA0014 airfoil. Xie and Song [4] developed a 3D Navier-Stokes solver to investigate the aerodynamic characteristics of flapping wing on the low speed and low Reynolds number.

These researches mentioned above have done much work on the flapping wing. And it is necessary to go further on the study about flapping wing. We aim to research the flapping wing air vehicle including the fuselage, vertical and horizontal stabilizers. Therefore, the chimera grid method is chosen to investigate the flapping wing air vehicle for the complex configuration. Firstly, we apply the chimera grid method on the flapping wing researching, and get some basic aerodynamic characteristics of flapping wing. The following are the main work of this paper.

In this work, a 3D Euler/RANS solver is developed for researching the aerodynamics of flapping wing. The chimera grids are used as the grid system including motion wing grid and stationary background grid. In order to deal with the preprocessing of chimera grid, an efficient method, namely distance-decreasing searching method, is developed to apply on the hole-cutting and the searching of interpolation cells. Then the research about the effect of angle of attack, reduced frequency, flapping angle, twisting angle, airfoil of cross section are performed.

2 Chimera Grids System

2.1 Chimera Grid Method

The chimera method is often used in complex configurations. In chimera grids, the flow domain is divided into several geometrically simple sub-domains in which independent meshes can be generated and different flow physics can be applied. Two main advantages [5] appear when overset meshes are used to discretize the computational domain: (1) the mesh generation is eased by reducing the

constraints on blocks shapes, and (2) moving bodies can be handled easily.

2.2 Flapping Wing Grids

In this paper, the chimera method is chosen for the numerical simulation of flapping wing. When using the chimera method, the wing grid can be generated once but distorts in unsteady calculation.

Fig.1 shows the grids used in this paper. The Fig.1a is the flapping wing in the neutral location, and Fig.1b is the flapping wing in the end of up stroke.

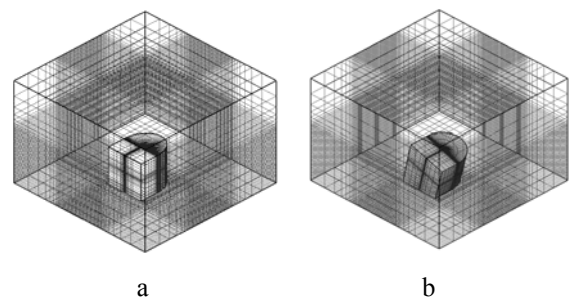


Fig.1 chimera grids of flapping wing

The topology of wing grid is CH with cell number $153 \times 25 \times 57$, and the background grid is Cartesian grid with cell number $91 \times 91 \times 57$. In the process of unsteady calculating, the wing grid distorts at every pseudo time step, but the background grid keep stationary all the time.

Because of the relative position of wing grid and background grid changes at every pseudo time step, the hole-cutting and searching of interpolation cells should be done at every pseudo time step.

A new method is developed for confirming corresponding cells between two overlapping grids, namely distance-decreasing searching method. The algorithm of distance-decreasing searching method can applied on hole-cutting and interpolation cells searching. Next subsections will introduce the algorithm and applications of distance-decreasing searching method.

2.3 Distance-Decreasing Searching Method

There is relative movement between background grid and wing grid, and the wing grid changes at every computing location for its

distortion, so the hole-cutting and grids interface communications are need at every computing location. An efficient method is developed to apply on the preprocessing of chimera grids, and the method is efficient, reliable and simple in hole-cutting and interpolation cells searching, namely distance-decreasing searching method.

Distance-decreasing searching method is based on the following thought: given a point A , and a successive structure grid region Ω , and a point B in region Ω , if point B is the closest point to point A in region Ω , these distances of points around point B to point A are all bigger than the distance of point B to point A ; if point B is not the closest point to point A in region Ω , there must be one point around point B is closer to point A than point B to point A . The algorithm is as following:

1. Given a point A , and a point B from structure grid region Ω , calculate the distance between point A and point B , denoted by l_{AB} .
2. Calculate the distance between point A and these points around point B ; then choose the nearest point to point A denoted by C , the distance between point A and point C is denoted by l_{AC} .
3. Compare the distance l_{AB} and l_{AC} , if $l_{AB} \leq l_{AC}$, the point B is the point nearest to point A in region Ω , stop searching; if $l_{AB} > l_{AC}$, let C replace point B , turn to step 2 and continue.

This process is the algorithm of distance-decreasing searching method, the name got because the distance between two points is decreasing till finding out the closest point.

Fig.2 is the sketch map of this method. This is an overlapping field of Cartesian grid and curvilinear grid.

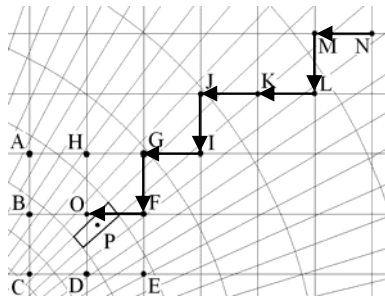


Fig.2 Sketch map of distance-decreasing searching method

When using the cell-center scheme finite volume method, the cell center value is need. Let P is an interpolated point in curvilinear grid; we aim to find out the interpolation donor cells in Cartesian grid, which are the cells $ABOH$, $BCDO$, $ODEF$ and $HOFG$. If the point O is found, the four donor cells are fixed. Any point will be chose as the beginning point, point N for example. Then, the path from N to O is $N \rightarrow M \rightarrow L \rightarrow K \rightarrow J \rightarrow I \rightarrow G \rightarrow F \rightarrow O$ using the distance-decreasing searching method.

In traditional way to search the target point, the quantity of searching points is $O(i \times j)$ in 2D grids, and $O(i \times j \times k)$ in 3D grids. (Here i, j, k are curvilinear grid cell numbers.) From the sketch map of Fig.2, we known the search of distance-decreasing searching method is on a curve, similar as linear search. The number of search points is less than 4 times the number of diagonal points in 2D grids, and 6 times the number of diagonal points in 3D grids. So the quantity of searching points of the distance-decreasing searching method is $O(4(i^2 + j^2)^{1/2})$ in 2D grids, and $O(6(i^2 + j^2 + k^2)^{1/2})$ in 3D grids. Therefore the search of this method is a quasi-linear search, so the distance-decreasing searching method has high efficiency when the cell number of grid is large.

Table 1 gives the CPU time cost comparison between used and unused distance-decreasing searching method in preprocessing of chimera grids in this paper. The frequency of CPU is 2.8G Hz of Intel Pentium 4. Next subsection will introduce the hole-cutting algorithm used distance-decreasing searching method.

Table 1 CPU time cost comparison between used and unused distance-decreasing searching method of chimera grids in this paper (s)

	Hole-cutting time	Interpolation cell searching time
Used distance-decreasing searching method	7.73	0.40
Unused distance-decreasing searching method	983.23	6.18

2.4 Hole-cutting

There are several hole-cutting methods, including: surface normal vector method [6], ray casting method [7], hole map method [8, 9], object X-rays method [7], and the others [10-12]. These algorithm are all complex, we develop a new hole-cutting method based on the distance-decreasing searching method, which is efficient and simple.

In the chimera grids composed from grid Ω_1 and Ω_2 , we use Ω_2 to cut hole in Ω_1 . The following is the hole-cutting algorithm based on the distance-decreasing searching method.

1. Choose original boundary in grid Ω_2 , denoted by C , which is a closure original boundary, composed of certain surface or some surfaces.

2. Choose a temporary center point P_0 in the original boundary.

3. Define the search circle, P_0 is the center, radius R_{max} is the maximum distance from the point P_0 to the point on surface C .

4. For any point P_1 falling in the search circle of grid Ω_1 , use distance-decreasing searching method to find out the nearest point P_2 in region Ω_2 . If the point P_2 is in the boundary C , set its tag IBLANK be 0 from 1.

After the process finished, all these points, whose tag IBLANK is 0, compose the hole-points in grid Ω_1 .

Using this method, we get the hole-cutting result of the flapping wing chimera grids in this paper. The original hole-boundary and the artificial hole- boundary are shown in Fig.3.

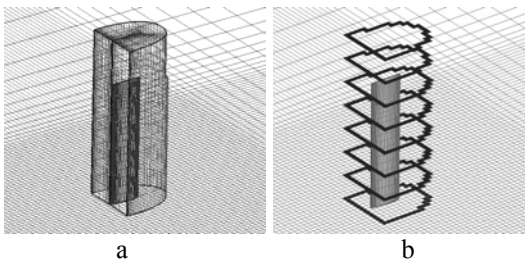


Fig.3 (a) Original hole-boundary and (b) Artificial hole-boundary

3 Numerical Method and Flapping Motion

A numerical method is developed to solve the Euler/Navier-Stokes equations for investigating the flowfields of the flapping wings based on chimera method. The spatial

discretization is characterized by a second-order cell-center method for finite volumes. A five-stage Runge-Kutta scheme is employed to achieve convergence of the solution by integration with respect to time. For unsteady flows an implicit dual time-stepping scheme is used. Implicit residual smoothing is employed to accelerate convergence. The Baldwin-Lomax algebraic turbulent model is applied for calculating the turbulence flows.

In chimera method, the trilinear interpolation is used in the grid interface communication.

The wing motion is compose of flapping and twisting. The flapping angle is defined as:

$$\psi(t) = \psi(z) \cos(\omega t) \quad (1)$$

The twisting angle is defined as:

$$\alpha(z, t) = \alpha_0 + \alpha_m(z) \cos(\omega t + \Phi) \quad (2)$$

$$\alpha_m(z) = \alpha_{m,tip} \times \frac{z}{b} \quad (3)$$

The reduce frequency is:

$$k = \frac{\omega c}{2U_\infty} \quad (4)$$

Here, the Ψ is the flapping angle, z the relative distance to root on the wing, α the twisting angle, α_0 the mean angle of attack, $\alpha_{m,tip}$ the twisting angle at wingtip, b the half span of the wing, Φ the phase shift between Ψ and α , ω the angular velocity, U_∞ the freestream velocity.

Fig.4 shows the wing geometry and motion parameters for the flapping wing.

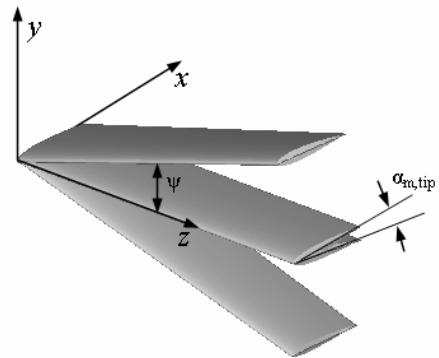


Fig.4 Wing geometry and motion parameters for the flapping wing

4 Computational Results

4.1 3D flapping wing in Euler equations

A numerical example is calculated for validation. Fig.5 are the plots of lift coefficient C_l and drag coefficient C_d vs. t/T of NACA0012 airfoil at the $\alpha_0=0^\circ$ and $\alpha_0=4^\circ$, respectively. And other parameters are: $\alpha_{m,tip}=4^\circ$, $M_\infty=0.3$, $A=8$, $\Psi=15^\circ$, $\Phi=90^\circ$, $k=0.1$, by Euler equation. In Fig.5 the computational results are in good agreement with the results of reference [13].

The direction of lift coefficient C_l is the same to the y axis, and the direction of drag coefficient C_d is the same to the x axis. The directions of thrust coefficient C_t is opposite to the x axis. The relationship between drag coefficient and thrust coefficient is $C_d=-C_t$.

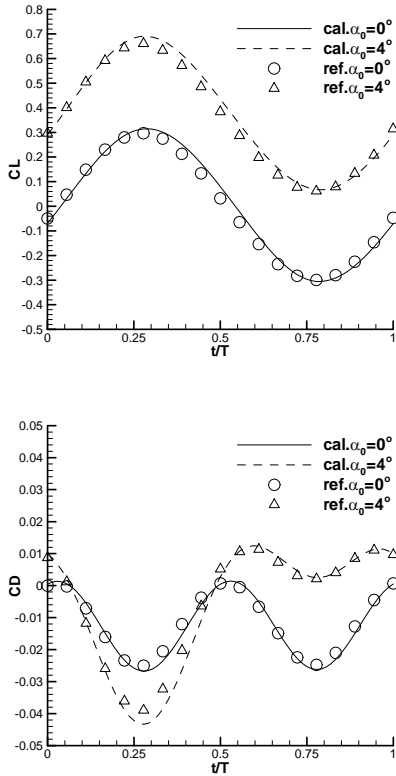


Fig.5 Plots of C_l and C_d coefficients vs. t/T at $\alpha_0=0^\circ, 4^\circ$ in Euler equations, and $\alpha_{m,tip}=4^\circ, M_\infty=0.3, A=8, \Psi=15^\circ, \Phi=90^\circ, k=0.1, NACA0012$

4.2 3D flapping wing in RANS equations

Fig.6 and Fig.7 is the result of C_l and C_d coefficients compare between Euler and RANS equations. The Reynolds number of RANS solution is 10^6 , the Baldwin-Lomax algebraic turbulent model is applied for calculating the turbulence flows, and the other parameters are the same with the Euler solution.

From the results of Fig.6 and Fig.7, the lift coefficient C_l got by RANS equations is a little less than which got by Euler equations. The drag coefficient C_d got by RANS equations is notably bigger than which got by Euler equations. The results accord with actual situation logically for the existence of viscosity.

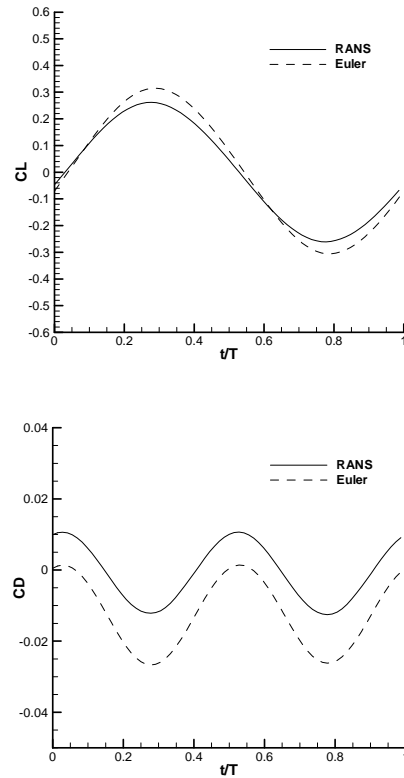
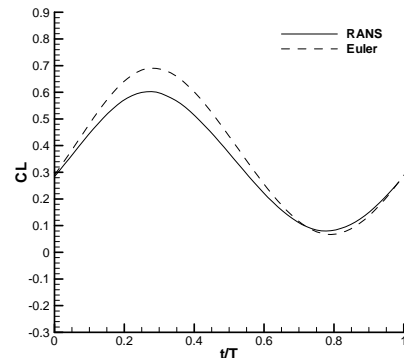


Fig.6 Plots of C_l and C_d coefficients vs. t/T at $\alpha_0=0^\circ$ in Euler and RANS equations, and $\alpha_{m,tip}=4^\circ, M_\infty=0.3, A=8, \Psi=15^\circ, \Phi=90^\circ, k=0.1, Re=10^6, NACA0012$



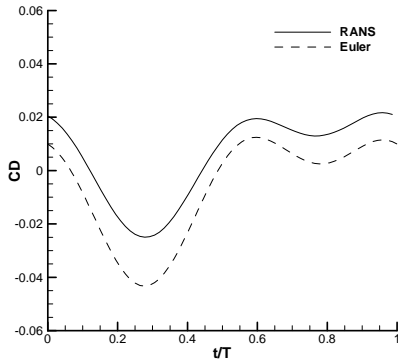


Fig.7 Plots of C_l and C_d coefficients vs. t/T at $\alpha_0=4^\circ$ in Euler and RANS equations, and $\alpha_{m,tip}=4^\circ$, $M_\infty=0.3$, $A=8$, $\Psi=15^\circ$, $\Phi=90^\circ$, $k=0.1$, $Re=10^6$, NACA0012

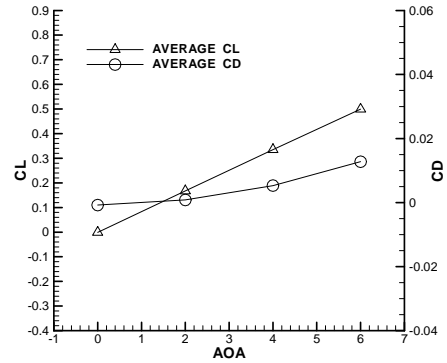


Fig.8 Plots of C_l and C_d coefficients vs. t/T at $\alpha_0=0^\circ, 2^\circ, 4^\circ, 6^\circ$ in RANS equations, and $\alpha_{m,tip}=4^\circ$, $M_\infty=0.3$, $A=8$, $\Psi=15^\circ$, $\Phi=90^\circ$, $k=0.1$, $Re=10^6$, NACA0012

4.3 Effect of angle of attack

Fig.8 and Fig.9 show the effect of angle of attack. The results show that the lift and drag coefficients increase with the increasing of angle of attack.

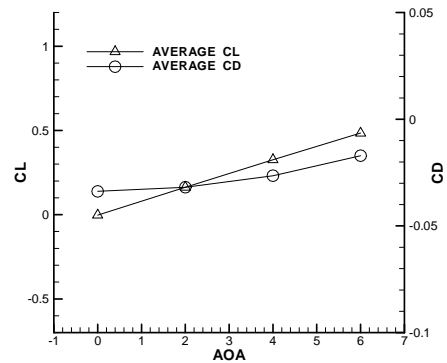
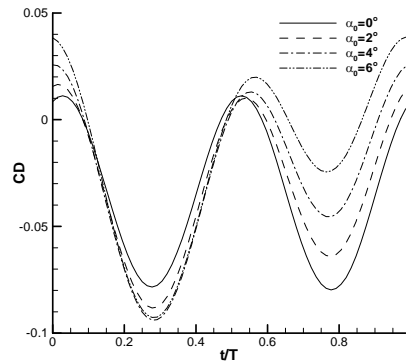
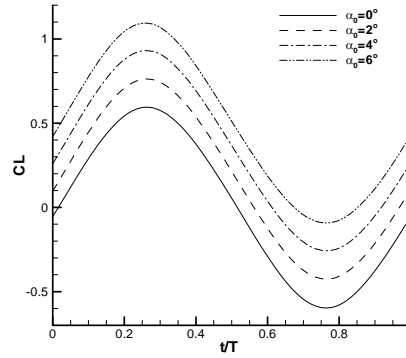
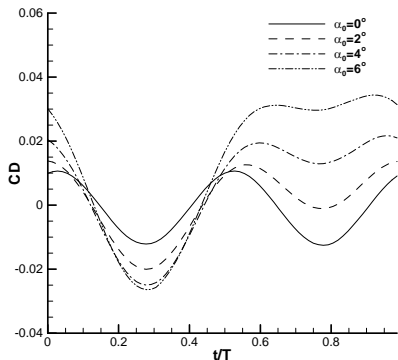
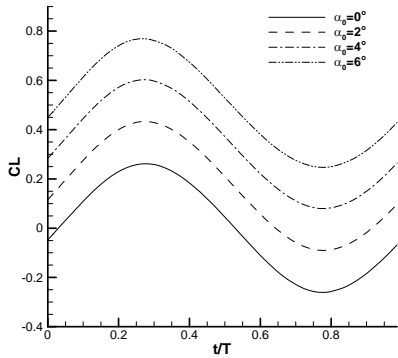


Fig.9 Plots of C_l and C_d coefficients vs. t/T at $\alpha_0=0^\circ, 2^\circ, 4^\circ, 6^\circ$ in RANS equations, and $\alpha_{m,tip}=4^\circ$, $M_\infty=0.3$, $A=8$, $\Psi=15^\circ$, $\Phi=90^\circ$, $k=0.2$, $Re=10^6$, NACA0012

4.4 Effect of reduced frequency

Fig.10 and Fig.11 show the effect of reduced frequency. The results show that the increasing of reduce frequency can decrease the drag coefficient which means increase the thrust coefficient, and increase the peak value range of lift coefficient in a circle, but affect average lift coefficient slightly.

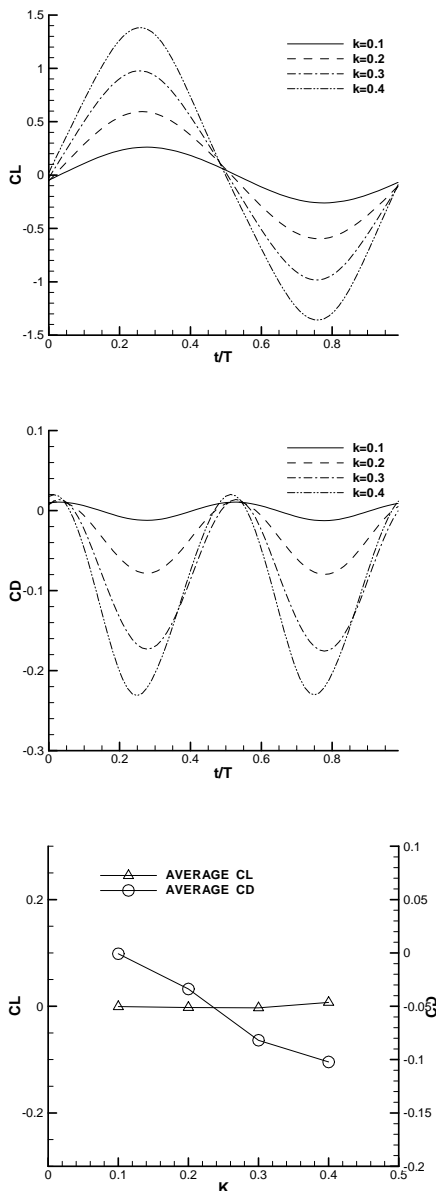


Fig.10 Plots of C_l and C_d coefficients vs. t/T at $k=0.1, 0.2, 0.3, 0.4$ in RANS equations, and $\alpha_0=0^\circ, \alpha_{m.tip}=4^\circ, M_\infty=0.3, A=8, \Psi=15^\circ, \Phi=90^\circ, Re=10^6, NACA0012$

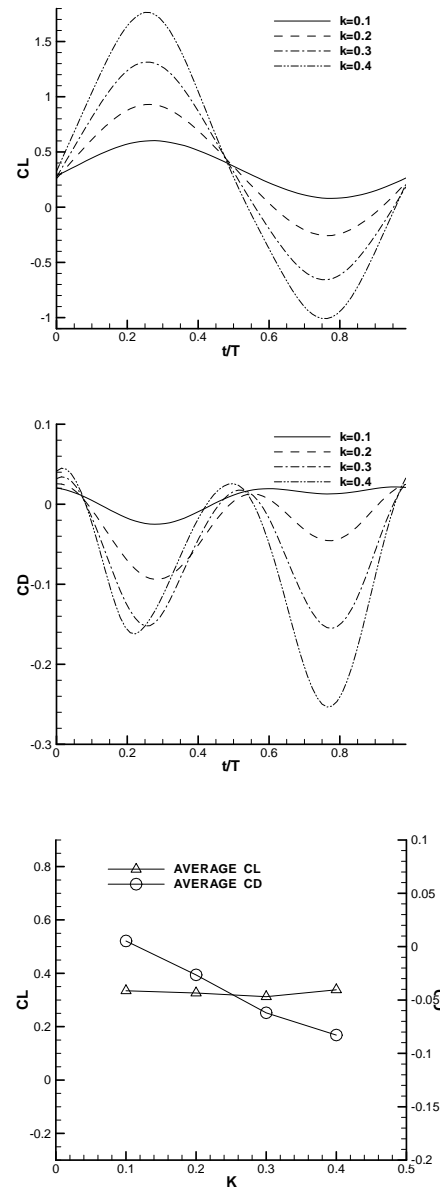


Fig.11 Plots of C_l and C_d coefficients vs. t/T at $k=0.1, 0.2, 0.3, 0.4$ in RANS equations, and $\alpha_0=4^\circ, \alpha_{m.tip}=4^\circ, M_\infty=0.3, A=8, \Psi=15^\circ, \Phi=90^\circ, Re=10^6, NACA0012$

4.5 Effect of flapping angle

Fig.12 and Fig.13 show the effect of flapping angle. The results show that the increasing of flapping angle can increase the thrust coefficient which means decrease the drag coefficient, and increase the peak value range of lift coefficient, but affect average lift coefficient slightly. The effect of flapping angle is similar with the reduced frequency.

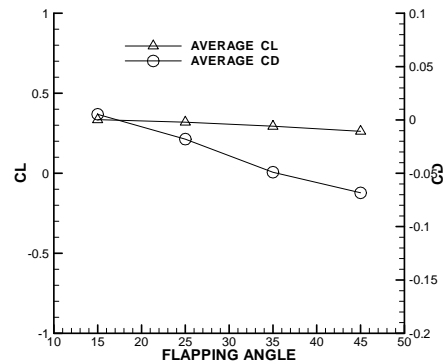
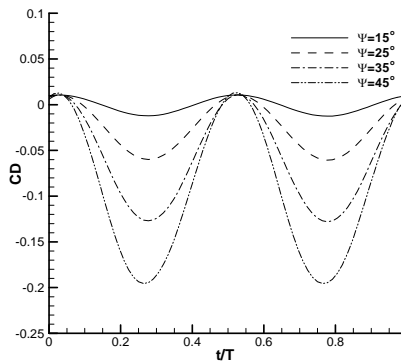
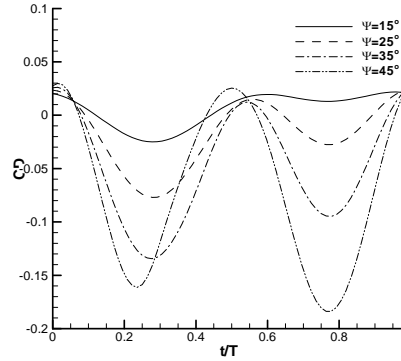
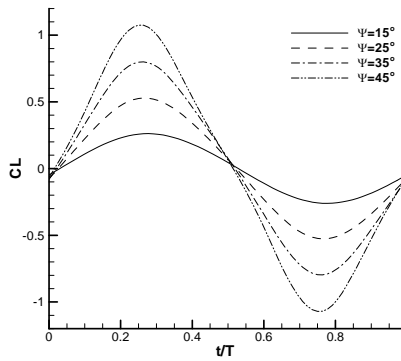


Fig.13 Plots of C_l and C_d coefficients vs. t/T at $\Psi=15^\circ$, 25° , 35° , 45° in RANS equations, and $\alpha_0=4^\circ$, $\alpha_{m,tip}=4^\circ$, $M_\infty=0.3$, $A=8$, $k=0.1$, $\Phi=90^\circ$, $Re=10^6$, NACA0012

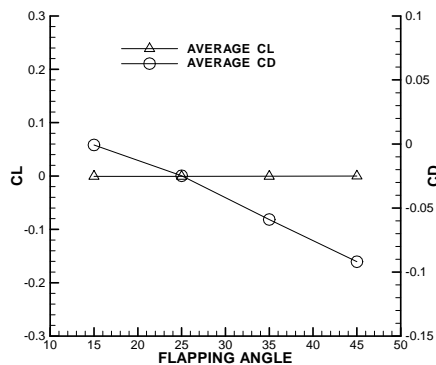
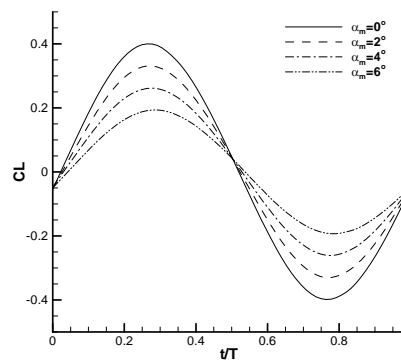
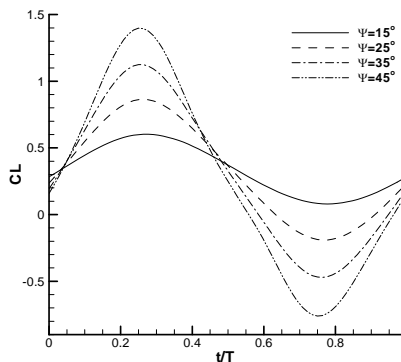


Fig.12 Plots of C_l and C_d coefficients vs. t/T at $\Psi=15^\circ$, 25° , 35° , 45° in RANS equations, and $\alpha_0=0^\circ$, $\alpha_{m,tip}=4^\circ$, $M_\infty=0.3$, $A=8$, $k=0.1$, $\Phi=90^\circ$, $Re=10^6$, NACA0012



4.6 Effect of twisting angle

Fig.14 and Fig.15 show the effect of twisting angle at the condition of $\Phi=90^\circ$. The increasing of twisting angle can decrease the peak value range of lift coefficient and increase the drag coefficient.

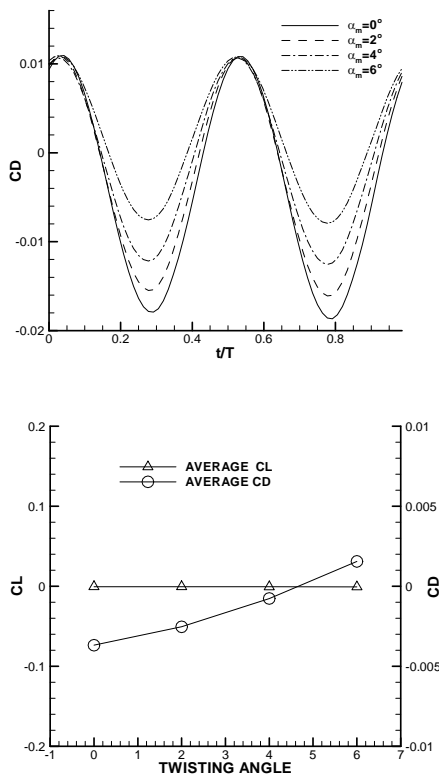


Fig.14 Plots of C_l and C_d coefficients vs. t/T at $\alpha_{m,tip}=0^\circ$, 2° , 4° , 6° in RANS equations, and $\alpha_0=0^\circ$, $\Psi=15^\circ$, $M_\infty=0.3$, $A=8$, $k=0.1$, $\Phi=90^\circ$, $Re=10^6$, NACA0012

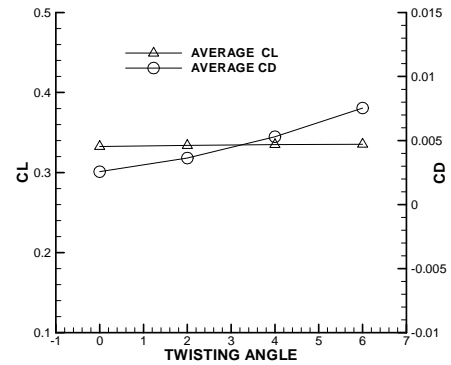
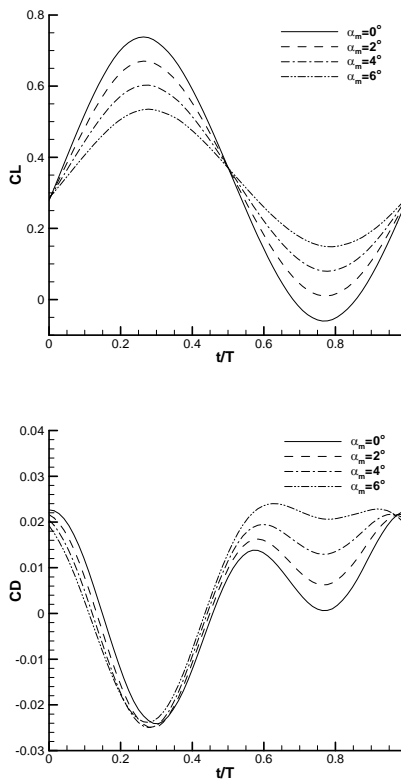
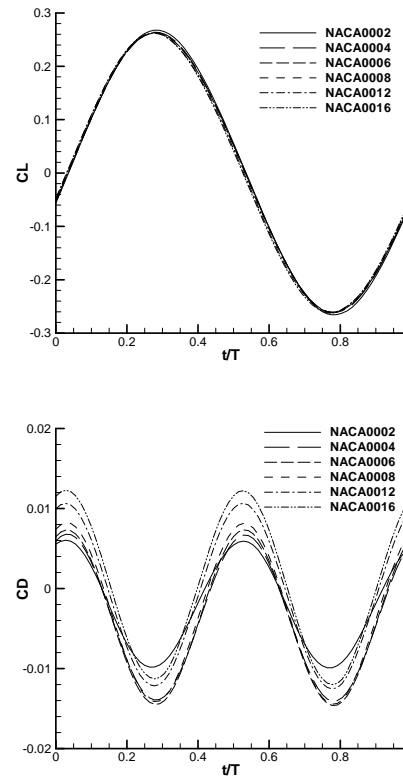


Fig.15 Plots of C_l and C_d coefficients vs. t/T at $\alpha_{m,tip}=0^\circ$, 2° , 4° , 6° in RANS equations, and $\alpha_0=4^\circ$, $\Psi=15^\circ$, $M_\infty=0.3$, $A=8$, $k=0.1$, $\Phi=90^\circ$, $Re=10^6$, NACA0012

4.7 Effect of airfoil thickness

Fig.16 and Fig.17 show the effect of airfoil thickness. The airfoil thickness has little effect on lift coefficient, but has obvious effect on thrust coefficients. The relationship between airfoil thickness and thrust coefficient is not monotony. Too thin or too thick airfoils both can not get big thrust coefficient.



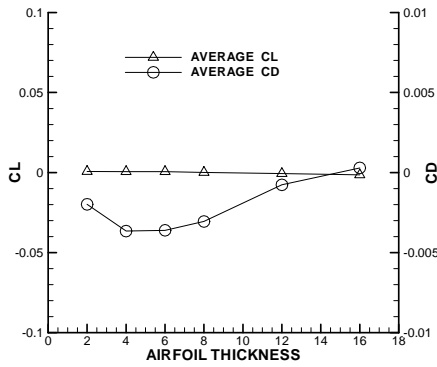


Fig.16 Plots of C_l and C_d coefficients vs. t/T at NACA0002, NACA0004, NACA0006, NACA0008, NACA0012, NACA0016 in RANS equations, and $\alpha_0=0^\circ$, $\alpha_{m.tip}=4^\circ$, $\Psi=15^\circ$, $M_\infty=0.3$, $A=8$, $k=0.1$, $\Phi=90^\circ$, $Re=10^6$

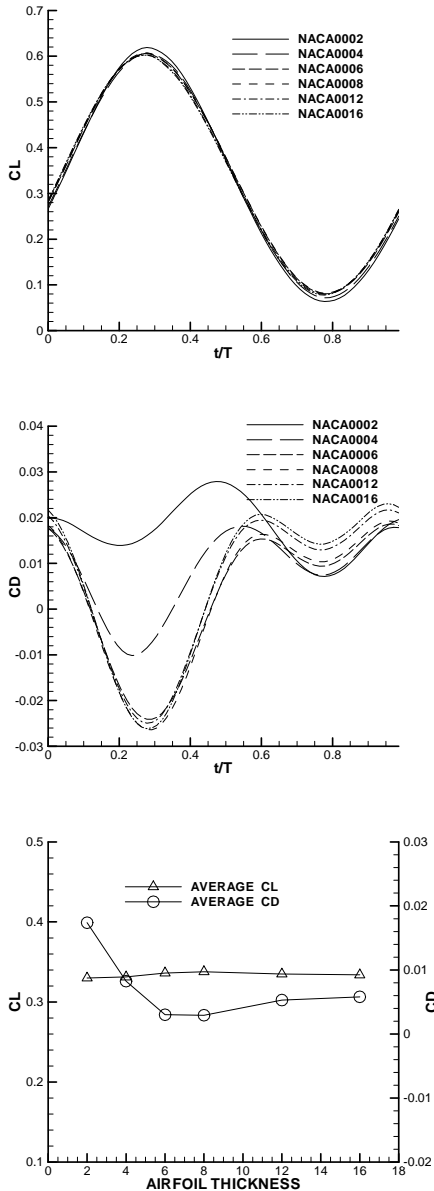


Fig.17 Plots of C_l and C_d coefficients vs. t/T at NACA0002, NACA0004, NACA0006, NACA0008, NACA0012, NACA0016 in RANS equations, and $\alpha_0=4^\circ$, $\alpha_{m.tip}=4^\circ$, $\Psi=15^\circ$, $M_\infty=0.3$, $A=8$, $k=0.1$, $\Phi=90^\circ$, $Re=10^6$

5 Conclusions

The aerodynamic characteristics of flapping wing are investigated by solving the Euler/RANS equations based on the chimera method. Some basic characteristics of flapping wing are researched, and some basic results are given.

The calculating results show that:

1. The method developed in this paper can be used to simulate the flapping wing. The method is reliable and practical.
2. The lift and thrust coefficients get by RANS is lower than the Euler equations because of the viscosity. The result accord with actual situation logically.
3. The increasing of angle of attack can increase the lift coefficient, but decrease the thrust coefficient.
4. The increasing of reduce frequency can increase the thrust coefficient, but effect average lift coefficient slightly, just increase the peak value range of lift coefficient.
5. The increasing of flapping angle affects the lift and thrust coefficient similarly as the increasing reduced frequency.
6. The increasing of twisting angle can decrease the peak value range of lift coefficient and decrease the thrust coefficient at the condition of $\Phi=90^\circ$.
7. The airfoil thickness has little effect on lift coefficient, but has obvious effect on thrust coefficients. The relationship between airfoil thickness and thrust coefficient is not monotony. Too thin or too thick airfoils both can not get big thrust coefficient.

References

[1] Neef M F and Hummel D. Euler Solutions for a Finite-Span Flapping Wing. *Fixed and Flapping Wing Aerodynamics for Micro Air Vehicle Applications*. Vol. 195, pp 429-451, 2001.

- [2] Tuncer I H and Platzer M F. Thrust Generation due to Airfoil Flapping. *AIAA Journal*. Vol. 34, No. 2, pp 324-331, February, 1996.
- [3] Lin S Y and Hu J J. Aerodynamic Performance Study of Flapping-Wing Flowfields. *23rd AIAA Applied Aerodynamics Conference*. 6-9 June, 2005. AIAA 2005-4611.
- [4] Xie H, Song W P and Song B F. Numerical solution of Navier-Stokes Equations for Flow over a Flapping Wing. *Journal of Northwestern Polytechnical University*. Vol. 26, No. 1, pp 104-109, February, 2008.
- [5] Juvigny X, Canonne E and Benoit C. Multigrid Algorithms for the Chimera Method. *42nd AIAA Aerospace Sciences Meeting and Exhibit*. 5-8 January, 2004. AIAA 2004-758.
- [6] Slotnick J P, Kandula M, Buning P G. Navier-Stokes Simulation of the Space Shuttle Launch Vehicle Flight Transonic Flowfield Using a Large Scale Chimera Grid System. AIAA 94-1860.
- [7] Meakin R L. Object X-Rays for Cutting Holes in Composite Overset Structured Grids. *15th AIAA computational fluid dynamics conference*. Anaheim, CA, AIAA 2001-2537.
- [8] Steger J. Notes on Composite Overset Grid Schemes – Chimera. *Dept Mech., Aero. And Mat. Eng.*, University of California, Davis, 1992.
- [9] Suhs N E, Rogers S E, Dietz W E. PEGASUS 5: An Automate Pre-Processor For Overset-Grid CFD. *AIAA Journal*. Vol. 41 (6), pp 1037-1045, 2003.
- [10] Li H T, Yan C. A New Method of Hole-point Search in Grid Embedding Technique. *Aerodynamics Journal*. Vol. 19 (2), pp 156-160, 2001.
- [11] Li X W, Fan X Q. Simulation of the Release of Store Based on the Moving Chimera Grid Technique. *Aerodynamics Journal*. Vol. 22 (1), pp 114-117, 2004.
- [12] Liu X, Lu L S. A Research on Overset Mesh Pre-processing Technology. *Computer Engineering and Application*. pp 23-36, January, 2006.
- [13] Neef M F, and Hummel D. Euler Solutions for a Finite-Span Flapping Wing. *Fixed and Flapping Wing Aerodynamics for Micro Air Vehicle Applications*. Vol. 195, pp 429-451, 2001.

Copyright Statement

The authors confirm that they, and/or their company or institution, hold copyright on all of the original material included in their paper. They also confirm they have obtained permission, from the copyright holder of any third party material included in their paper, to publish it as part of their paper. The authors grant full permission for the publication and distribution of their paper as part of the ICAS2008 proceedings or as individual off-prints from the proceedings.